Following the excited state relaxation dynamics of indole and 5-hydroxyindole using time-resolved photoelectron spectroscopy

Cite as: J. Chem. Phys. **135**, 194307 (2011); https://doi.org/10.1063/1.3659231
Submitted: 26 August 2011 . Accepted: 19 October 2011 . Published Online: 17 November 2011

Ruth Livingstone, Oliver Schalk, Andrey E. Boguslavskiy, Guorong Wu, L. Therese Bergendahl, Albert Stolow, Martin J. Paterson, and Dave Townsend

Following the excited state relaxation dynamics of indole and 5-hydroxyindole using time-resolved photoelectron spectroscopy

Ruth Livingstone,[1] Oliver Schalk,[2] Andrey E. Boguslavskiy,[2] Guorong Wu,[2]
L. Therese Bergendahl,[1] Albert Stolow,[2] Martin J. Paterson,[1] and Dave Townsend[1,a)]
[1]*School of Engineering and Physical Sciences, Heriot-Watt University, Edinburgh EH14 4AS, United Kingdom*
[2]*Steacie Institute for Molecular Sciences, National Research Council of Canada, Ottawa, Ontario K1A 0R6, Canada*

(Received 26 August 2011; accepted 19 October 2011; published online 17 November 2011)

Time-resolved photoelectron spectroscopy was used to obtain new information about the dynamics of electronic relaxation in gas-phase indole and 5-hydroxyindole following UV excitation with femtosecond laser pulses centred at 249 nm and 273 nm. Our analysis of the data was supported by *ab initio* calculations at the coupled cluster and complete-active-space self-consistent-field levels. The optically bright ^1L_a and ^1L_b electronic states of $^1\pi\pi^*$ character and spectroscopically dark and dissociative $^1\pi\sigma^*$ states were all found to play a role in the overall relaxation process. In both molecules we conclude that the initially excited ^1L_a state decays non-adiabatically on a sub 100 fs timescale via two competing pathways, populating either the subsequently long-lived ^1L_b state or the $^1\pi\sigma^*$ state localised along the N-H coordinate, which exhibits a lifetime on the order of 1 ps. In the case of 5-hydroxyindole, we conclude that the $^1\pi\sigma^*$ state localised along the O-H coordinate plays little or no role in the relaxation dynamics at the two excitation wavelengths studied. © *2011 American Institute of Physics*. [doi:10.1063/1.3659231]

I. INTRODUCTION

Over the course of billions of years of evolution, specific molecules have been selected for use as the "building blocks" of life. One such example of this is found in melanins, the group of pigments found in animals, plants, and humans. The most common form of melanin in humans is eumelanin which colours the skin, hair, and retina and serves to protect the body from the potentially damaging effects of ultraviolet (UV) radiation. Eumelanin is a complex polymer made up of three main building blocks; 5,6-dihydroxyindole (DHI), indolequinone (IQ), and 5,6-dihydroxyindole-2-carboxylic acid (DHICA),[1–3] the structures of which are shown in Figure 1. More detailed insight into the relaxation dynamics of the electronically excited states that are populated in these different molecules following absorption of UV radiation would help reveal the response of melanin pigments to photoexcitation and the subsequent mechanisms for dissipation of excess energy.

If one wishes to begin studying the photophysics of melanin in a systematic way, one strategy is to start with a relatively simple model and then gradually incorporate additional substituent groups. As can be seen from Figure 1, indole provides a first approximation to all three of the principal constituent units of eumelanin and, as such, it provides a useful starting point for an investigation into electronic relaxation in this important class of biological systems. As a next step up in complexity one may then also begin to consider the 5-hydroxyindole molecule. By comparing the relaxation dynamics in these two species, it should be possible to gain insight into the role of the hydroxyl group in the full melanin system.

The electronic spectroscopy of indole in the gas phase has been well studied and photoexcitation in the 285–220 nm region is primarily to two valence states of $^1\pi\pi^*$ character and $^1A'$ symmetry which are historically labelled ^1L_a and ^1L_b.[4] At energies above ~220 nm, strong absorption to two higher lying $^1\pi\pi^*$ states, denoted ^1B_a and ^1B_b, also becomes significant.[5–7] The region around the ^1L_b origin (which lies at 283.8 nm) has been investigated extensively[8–18] and numerous vibronic bands are observed up to ~271 nm. Since no individual vibronic progression exhibits more than two members, the geometries of the S_0 ground state and the ^1L_b state are assumed to be similar. At shorter excitation wavelengths the spectrum becomes increasingly unstructured due to the onset of excitation to the ^1L_a state, the origin of which is believed to be located very close to 273 nm although it has not been observed directly.[19,20] The lack of observable vibronic structure in the ^1L_a state may be attributed to its short lifetime and this may be rationalised, at least in part, on the basis of results from a recent comprehensive theoretical and experimental study by Schmitt and co-workers.[18,21] These authors conclude that the ^1L_a state origin is very close to a conical intersection that connects to the ^1L_b state, mediated by Herzberg-Teller active modes. This process is essentially barrierless and so vibrationally excited ^1L_a states that are accessed radiatively, funnel directly through into the ^1L_b minimum. Vibronic coupling between the ^1L_a and ^1L_b states (inferred from analysis of the transition dipole moment orientation) also accounts for some of the observed decreases in the ^1L_b state lifetime, which falls from 17.5 ns at the electronic origin to as short as 3–4 ns at around 276 nm. In addition, the anomalously short lifetime of a vibronic

a)Author to whom correspondence should be addressed. Electronic mail: D.Townsend@hw.ac.uk.

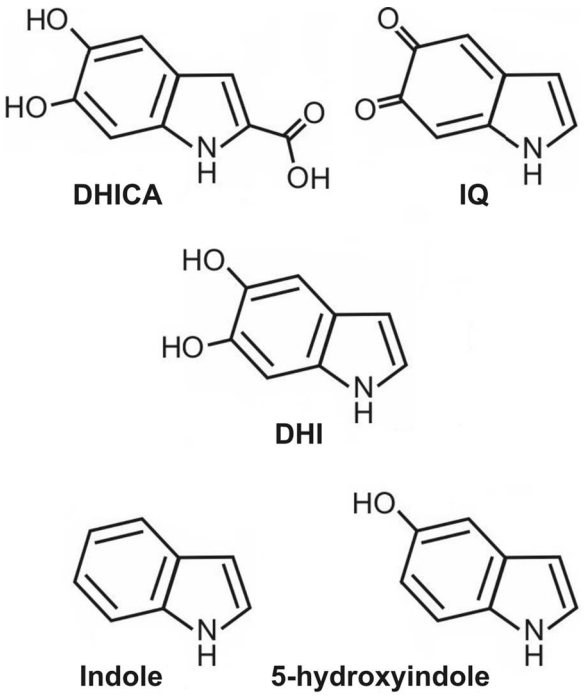

FIG. 1. Diagrams of the three constituent building blocks of eumelanin: 5,6-dihydroxyindole-2-carboxylic acid (DHICA), indolequinone (IQ), and 5,6-dihydroxyindole (DHI). Also depicted are indole and 5-hydroxyindole, which are the two molecules used in the present study.

band lying just 316 cm^{-1} above the ^1L_b origin, assigned as an out-of-plane mode, was attributed to coupling to an additional, dissociative electronic state of $^1\pi\sigma^*$ character. Such $^1\pi\sigma^*$ states are now recognised as a common feature in the excited state relaxation dynamics of many molecules containing NH and OH groups, and a number of systems have been extensively studied both experimentally and theoretically over the last decade. The recent review of Ashfold *et al.* (and references therein) provides an excellent starting point for an overview of these investigations.[22] In the case of indole, the $^1\pi\sigma^*$ state has been identified as having $^1A''$ symmetry and significant Rydberg (3s) character, with much of the electron density being localised on the NH group and exhibiting a node along the N-H bond.[23–25] The $^1\pi\sigma^* \leftarrow S_0$ transition possesses little or no oscillator strength and so is essentially "optically dark" to single photon absorption. Calculations from Sobolewski and Domcke using multireference *ab initio* methods have suggested that the threshold for internal conversion via a conical intersection connecting the optically bright $^1\pi\pi^*$ states to this $^1\pi\sigma^*$ state lies at around 5 eV (248 nm) above the ground state and is located along the N-H stretching coordinate.[24–26] The coupling is mediated by out-of-plane vibrational modes of a″ symmetry.[27] These authors also proposed that a second conical intersection, at more extended N-H bond distances, may then give rise to a mechanism for ultrafast internal conversion back to the electronic ground state, providing a fast non-radiative pathway for the disposal of excess absorbed UV energy. Alternatively, N-H bond fission may occur directly on the $^1\pi\sigma^*$ potential energy surface. The extremely rapid decay of the ^1L_a state via the $^1\pi\sigma^*$ route may also account, in part, for the lack of much observed vibronic structure in the indole absorption spectrum above the ^1L_a origin.

In recent years there have been various experimental studies that have sought to investigate the role of the $^1\pi\sigma^*$ state in indole, although there is a clear lack of consistency in the conclusions that have been reached. Zwier and co-workers recorded fluorescence dip infrared spectra following UV excitation of several ^1L_b vibronic bands between 283.8 nm and 272.9 nm.[28] Upon observing no significant change in the N-H stretching frequency relative to the ground state, it was concluded that coupling to the $^1\pi\sigma^*$ state does not play a major role in indole at these wavelengths. Evidence of $^1\pi\sigma^*$ involvement was, however, observed in several indole derivatives. This was attributed to the fact that the $^1\pi\sigma^*$ state is highly polar ($\mu = 11.0$ D) (Ref. 25) and therefore susceptible to large energy shifts relative to the much less polar ^1L_b state ($\mu = 1.55$ D), which may significantly modify the dynamics at similar excitation wavelengths.

Lee and co-workers employed multimass ion imaging techniques to study the photofragment translational energy distribution of the indolyl radical produced following excitation and subsequent dissociation of indole at 248 nm and 193 nm.[29] At both wavelengths they observed a bimodal translational energy distribution and concluded that the high kinetic energy component was the result of direct dissociation via the $^1\pi\sigma^*$ state following internal conversion from the initially prepared $^1\pi\pi^*$ states (which are predominantly ^1L_a at 248 nm and $^1B_a/^1B_b$ at 193.3 nm). The low kinetic energy component was attributed to a "statistical" unimolecular decay following internal conversion to the (highly vibrationally excited) ground electronic state. Similar findings were also reported by Ashfold and co-workers using H (Rydberg) atom photofragment translational spectroscopy at excitation wavelengths of 193.3 nm and between 240 and 285 nm.[30] The onset of a structured high kinetic energy H atom elimination channel, attributed to direct dissociation of the $^1\pi\sigma^*$ state along the N-H coordinate, was observed at excitation wavelengths shorter than 263 nm, with low kinetic energy H atoms being assigned to the decay of the indole S_0 ground state. Recent work by Stavros and co-workers employing femtosecond pump-probe spectroscopy also observed a bimodal H atom energy distribution following excitation at 200 nm.[31] These authors noted that the time constant for the appearance of the H atom photofragments was <200 fs in both elimination channels. They assigned the high kinetic energy component to direct dissociation via a $^1\pi\sigma^*$ state following relaxation from the initially excited $^1\pi\pi^*$ state ($^1B_a/^1B_b$) but were unsure of the source of the low kinetic energy signal, as the timescale was significantly shorter than that expected for statistical unimolecular decay from the vibrationally excited ground state.

In contrast to experiments interrogating the photoproducts formed following indole excitation, time-resolved measurements probing the decay of the initially excited states have reached somewhat different conclusions: Radloff and co-workers performed experiments on indole employing femtosecond pump-probe spectroscopy with coincidence detection of photoions and photoelectrons.[32] Their results suggested that, following excitation at 250 nm and 263 nm, the initially prepared $^1\pi\pi^*$ state(s) of indole have a lifetime

greater than several hundred picoseconds. Since the short time dynamics that might be expected for rapid internal conversion to the $^1\pi\sigma^*$ state were not observed, it was concluded that no significant coupling to this state was present at these pump wavelengths. Work by Zewail and co-workers using ultrafast electron diffraction also concluded that, following excitation at 267 nm, the $^1\pi\sigma^*$ state does not play a major role in the indole relaxation dynamics.[33] A decaying signal with a time constant of 6.3 ps, was attributed to the initially excited ^1L_a state relaxing via sequential couplings to lower lying $T_2(^3\pi\pi^*)$ and $T_1(^3\pi\pi^*)$ states. These authors also speculated that the $T_1(^3\pi\pi^*)$ state may then be responsible for subsequent H atom loss. Although, given El Sayed's rules,[34] the intersystem crossing (ISC) involved would be expected to take place on a much slower timescale than that observed, the calculated non-planar geometry of the T_2 state was used to argue that vibronic coupling could lead to a significantly increased ISC rate.

In contrast to indole, very little has been reported about the spectroscopy and dynamics of the 5-hydroxyindole molecule in the gas phase. *Ab initio* calculations have determined the two lowest lying optically excited states to be of $^1\pi\pi^*$ character, with ^1L_a lying above ^1L_b as is the case in indole.[35,36] The position of the ^1L_b origin sits at 303.9 nm and 305.9 nm for the gauche- and anti-conformers respectively, and at both these excitation wavelengths, as well as in the region between 290 and 295 nm, the fluorescence lifetime has been reported as 11.1 ns.[37–39] The development of a detailed understanding of the electronic relaxation dynamics of 5-hydroxyindole has, however, very recently taken a major step forward as a consequence of work performed by Ashfold and co-workers.[40] By employing a similar experimental methodology to their previous studies on indole, this group compared the H (Rydberg) atom photofragment translational distributions obtained from hydroxyindole and methoxyindole, substituted at both the 4- and 5-positions, over a range of excitation wavelengths between 303.9 nm and 193.3 nm. Equation of motion coupled cluster theory including single and double excitations (EOM-CCSD) and CASPT2 calculations were also employed to assist in interpreting the roles of N-H and O-H bond dissociation in the excited state relaxation dynamics. In the case of 4-hydroxyindole, O-H bond fission was found to be the dominant source of high kinetic energy H atoms at all excitation wavelengths studied. For 5-hydroxyindole, a very different behaviour was observed: high kinetic energy H atoms, originating predominantly from N-H bond fission (as determined by direct comparison with data from 5-methoxyindole) were observed at excitation wavelengths shorter than 255 nm, with some small contributions from O-H dissociation only becoming apparent below 235 nm. Excitation at wavelengths longer that 255 nm produced only low kinetic energy H atom fragments. The significant differences in the photodissociation dynamics exhibited by the 4- and 5-substituted systems was rationalised in terms of their different underlying electronic structures, with the role of the O atom p_x orbital being of particular relevance.

Here we present a study of the electronic relaxation dynamics of indole and 5-hydroxyindole in the gas-phase using time-resolved photoelectron spectroscopy (TRPES) in conjunction with *ab initio* calculations of the geometries and excited state potential surfaces of these molecules. The TRPES approach has a high sensitivity to the dynamics of electronic relaxation in molecular systems and our data offer new insight into the photophysics of this important class of model biological species. In contrast to previous time-resolved studies, we are able to directly observe the initially prepared ^1L_a state decaying on an ultrafast timescale via internal conversion to both the ^1L_b and $^1\pi\sigma^*$ states. We also conclude that the OH group in 5-hydroxyindole plays a minimal role in the relaxation process at the excitation wavelengths studied.

II. EXPERIMENTAL

Indole (≥99%) and 5-hydroxyindole (97%) were purchased from Sigma-Aldrich and used without further purification. Preliminary UV-Vis absorption spectra of the two molecules were recorded using a Varian 5e-spectrometer, evaporating the samples in a 1 cm long quartz cuvette at 80 °C. Our main experimental set-up employs a "magnetic bottle" photoelectron spectrometer which has previously been described in detail in Refs. 41 and 42. The solid samples were brought into the gas phase using a high intensity skimmed pulsed supersonic molecular beam (1 kHz Even-Lavie valve, 200 μm diameter conical nozzle).[43] Samples were held in a cartridge mounted within the valve body, directly behind the exit nozzle and heated by an external controller. Helium with a pressure of around 5 bar was used as a carrier gas and the samples were cooled via supersonic expansion into the source chamber of a differentially pumped ultra-high vacuum system. Our choice of carrier gas and expansion conditions means that we do not expect any significant formation of van der Waals complexes.[9] After travelling through a skimmer into a second interaction chamber, the sample beam was intersected at 90° by co-propagating UV pump and probe pulses. These pulses were produced using the signal outputs from two identical optical parametric amplifiers (TOPAS, Light Conversion). The 800 nm input for both TOPAS systems was provided by a Ti:Sapphire regenerative amplifier (Positive Light, Spitfire) pumped by two 1 kHz Nd:YLF lasers (Positive Light, Evolution) and seeded by a Ti:Sapphire oscillator (Spectra Physics, Tsunami) pumped by two Nd:YLF diode lasers (Spectra Physics, Millennia). The pump pulses (249 nm or 273 nm) were generated by mixing the signal output of one TOPAS with the 800 nm laser fundamental in a BBO-crystal and then subsequently doubling the generated sum frequency. The probe beam (300 nm or 320 nm) was obtained by generating the fourth harmonic of the second TOPAS signal beam output using successive doubling in two BBO crystals. Pulse energies for both pump and probe pulses were attenuated to ~1.3 μJ.

The temporal delay between the pump and the probe was precisely controlled using a motorized linear translation stage (Newport, ILS250PP) and driver (Newport, ESP300). A typical data collection run consisted of stepping the translation stage repeatedly between pump-probe delays of −500 fs to +500 fs in 50 fs increments and 40 exponentially increasing steps between +500 fs and +50 ps. The pump and probe were combined on a dichroic mirror and focussed into the

interaction region inside the vacuum chamber using a concave spherical aluminium mirror (f/150 for the pump and f/125 for the probe pulse, ensuring a smaller spot size of the probe pulse in the interaction region). Photoelectrons were detected by a microchannel plate (MCP) detector positioned at the end of the magnetic bottle flight tube. The pump-probe cross correlation width was around 180 fs. This measurement was obtained directly inside the vacuum chamber from non-resonant, two-colour (1 + 1′) multiphoton ionisation of Diazabicyclo[2,2,2]octane (DABCO) when the pump beam was 249 nm, and Azabicyclo[2,2,2]undecane (ABCU) when it was 273 nm. At each delay position, the time invariant one-colour pump alone and probe alone background photoelectron signals were dynamically subtracted from the pump-probe signal.

III. RESULTS

A. Calculations

The ground state geometries of indole and 5-hydroxyindole were optimized using density functional theory (B3LYP functional) in conjunction with the aug-cc-pVDZ basis set. Vertical excitation energies and oscillator strengths were calculated using EOM-CCSD;[44] this is equivalent to linear response (LR) coupled cluster theory for excitation energies. The effect of triples excitations were determined using the CCR(3) method,[45] which gives a non-iterative perturbative correction to LR-CCSD excitation energies, such that excitation energies for singly excited states are correct through third order in the fluctuation potential. The aug-cc-pVDZ basis was used for all coupled-cluster calculations. GAUSSIAN (Ref. 46) was used for the B3LYP and EOM-CCSD calculations, while the DALTON program[47] was used for the LR-CCSD and CCR(3) calculations. The carbon and nitrogen core 1s orbitals were frozen in the correlated calculations. The vertical excitation energies and oscillator strengths are shown in Table I. The values obtained reproduce the same state ordering as previous calculations and the relative state energies are also in good agreement.[26,40] The ^1L_a and $^1\pi\sigma^*_{NH}$ states undergo relatively small changes in energetic position upon hydroxylation whereas the ^1L_b state experiences a significant redshift, in excess of 0.3 eV. Figure 2 shows qualitative orbital representations of the nature of the various excited electronic states. The dominant contribution to the excited state is given by the value of ^Rc_i, which is the coefficient of the illustrated orbital transition in the right hand eigenvector of the EOM state.[44] The orbital transitions shown are the most important contributions to each state by at least a factor of 5 in all cases. The ^1L_a transition originates predominantly from the HOMO, whereas the $^1\pi\sigma^*$ and ^1L_b transitions originate predominantly from the HOMO-1. For the case of 5-hydroxyindole there are two distinct states of $^1\pi\sigma^*$ character with electron density separately localised on the NH and OH groups. Rigid scans along the N-H and O-H dissociation coordinates were performed using EOM-CCSD for the ground state, and the ^1L_a, ^1L_b, and $^1\pi\sigma^*_{NH}$ excited electronic states for indole, and those states plus the $^1\pi\sigma^*_{OH}$ state for 5-hydroxyindole. These are plotted in Figure 3. For the case of indole, EOM-CCSD for N-H dissociation on the $^1\pi\sigma^*$ state predicts a 0.46 eV barrier with the maximum is located at 1.4 Å, in good agreement with a recent calculation by Sobolewski and Domcke.[26] A very similar barrier is also present for the $^1\pi\sigma^*_{NH}$ state of 5-hydroxyindole, located at 1.3 Å. For the case of the $^1\pi\sigma^*_{OH}$ state the barrier is somewhat smaller, being just in excess of 0.1 eV, and is located at ∼1.2 Å. These results are also in good agreement with the recent work of Ashfold and co-workers.[40] Complete-active-space self-consistent-field (CASSCF) calculations were also performed, using GAUSSIAN,[46] to generate qualitatively correct wavefunctions in regions of strong non-adiabatic coupling. An active space consisting of 12 electrons in 11 orbitals was used, which generated 106953 singlet configurations. The basis used for CASSCF calculations was 6-31+G(d). Conical intersection searches were performed between the S_0 and $^1\pi\sigma^*$ states, the $^1\pi\pi^*$ and $^1\pi\sigma^*$ states, and the two lowest $^1\pi\pi^*$ states for indole. In the CASSCF calculations the two lowest $^1\pi\pi^*$ states correspond to ^1L_a and ^1L_b, however, we note that the relative ordering of these states is highly sensitive to dynamical electron correlation. Moreover, at distorted non-planar geometries the states mix heavily and the ^1L_a and ^1L_b labels lose significance. Orbital rotation derivatives were ignored in the solution to the coupled perturbed multi-configuration self-consistent field equations, due to the size of the active space. Additionally, symmetry restricted CASSCF was used to optimize the geometry of the $^1\pi\sigma^*$ state. This gave an equilibrium N-H bond length of 1.02 Å. Minimum energy crossing points (MECP) in the seam of intersection were obtained for all three pairs of states, and the geometries and branching space vectors for these are shown in Figure 4. The branching space defines the two directions in which

TABLE I. Vertical excitation energies (in eV) for indole and 5-hydroxyindole obtained from coupled cluster response theory in conjunction with an aug-cc-pVDZ one-electron basis set. Linear response CCSD (LR-CCSD), equivalent to EOM-CCSD, and CCR(3), which includes non-iterative triples effects are shown. The oscillator strengths *f* are also given, obtained from LR-CCSD.

	Indole			5-hydroxyindole		
State	LR-CCSD	CCR(3)	*f*	LR-CCSD	CCR(3)	*f*
$^1\pi\pi^*$ ^1L_b ($^1A'$)	4.823	4.762	0.0280	4.539	4.458	0.0636
$^1\pi\pi^*$ ^1L_a ($^1A'$)	5.241	5.117	0.1018	5.204	5.087	0.1223
$^1\pi\sigma^*_{NH}$ ($^1A''$)	5.046	5.017	0.0022	4.945	4.930	0.0000
$^1\pi\sigma^*_{OH}$ ($^1A''$)	...	...	...	5.063	5.045	0.0003

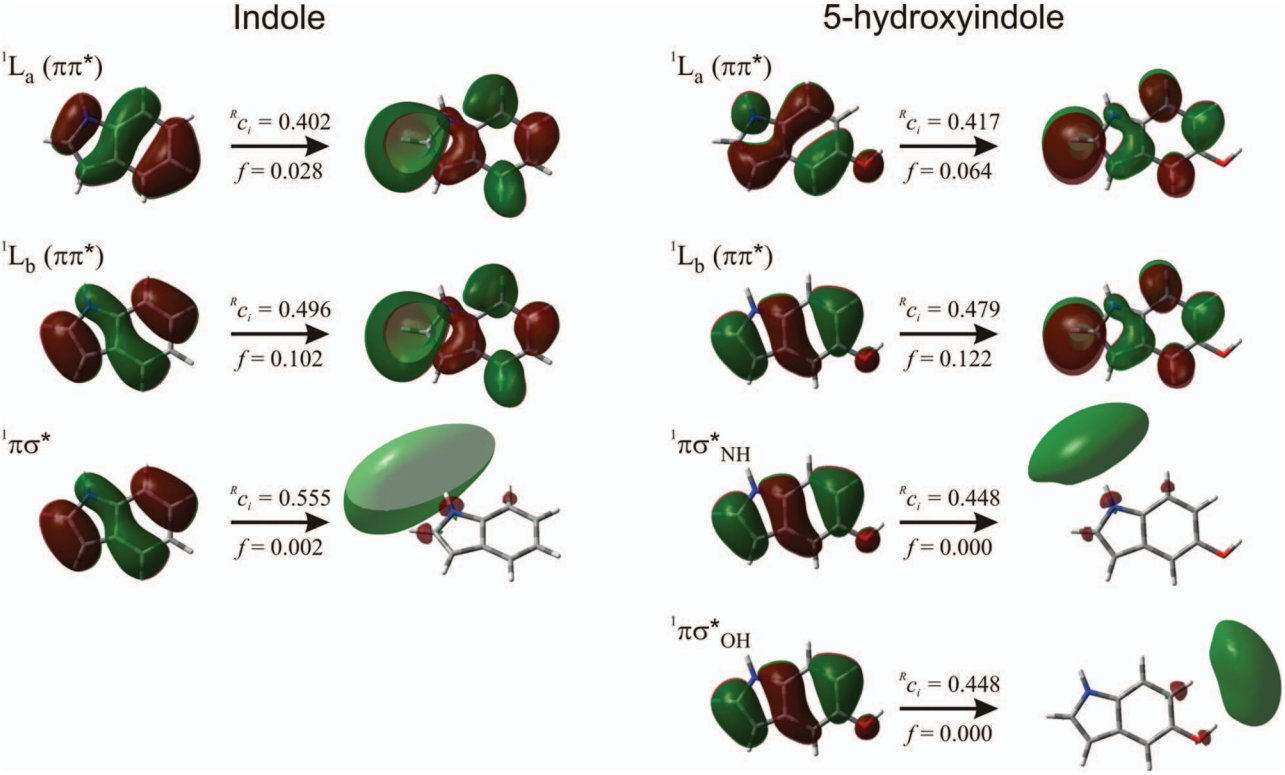

FIG. 2. Primary orbitals involved in transitions to ^1L_a, ^1L_b, and $\pi\sigma^*$ states for indole and 5-hydroxyindole. The magnitude of the EOM-CCSD amplitude, ^Rc_i, is shown. This reflects the importance of this orbital transition to the overall state, as discussed in more detail in the main text. The oscillator strength f is also shown for each transition.

nuclear motion lifts the degeneracy of the electronic states upon movement through a given conical intersection. In the case of the S_0 and $^1\pi\sigma^*$ states the MECP corresponds to a highly extended N-H bond distance of 1.8 Å, consistent with previous calculations.[24–26] The branching space here corresponds primarily to motion of the N and H atoms, with some component directed out of the plane of the indole ring. The $^1\pi\pi^*$ and $^1\pi\sigma^*$ states cross at an N-H bond distance of 1.2 Å at the MECP. The branching space is similar to the $S_0/^1\pi\sigma^*$ conical intersection, though involving a greater in-plane distortion of the pyrole moiety within the indole ring system. The MECP between the two lowest lying $^1\pi\pi^*$ states involves out-of-plane motions of the N-H and adjacent C-H bonds. The branching space for this conical intersection,

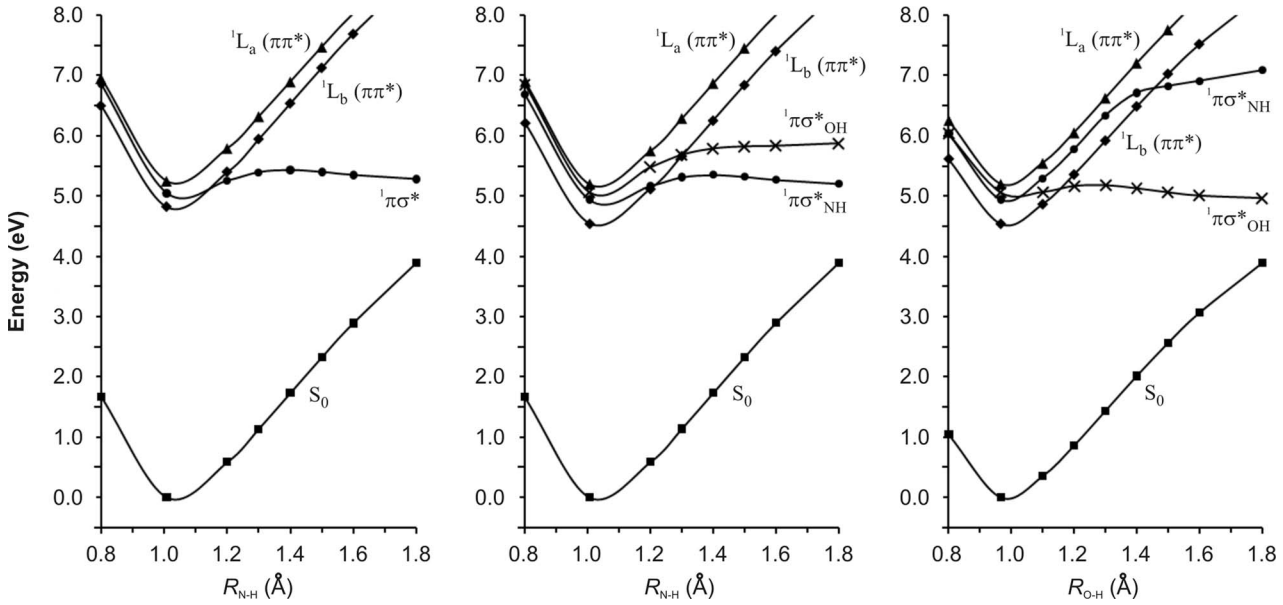

FIG. 3. Energy cuts, as obtained using EOM-CCSD/aug-cc-pVDZ for indole along the N-H coordinate and 5-hydroxyindole along both the N-H and O-H coordinates.

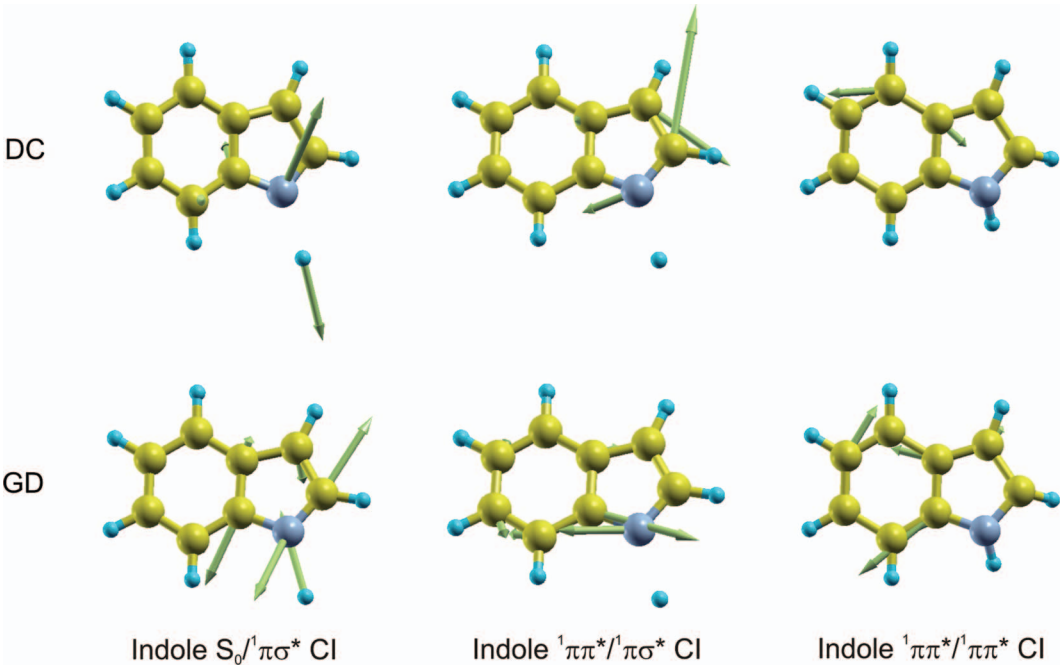

FIG. 4. Branching space vectors as obtained from CASSCF calculations in indole for the three conical intersections shown. The derivative coupling vector (DC) and the gradient difference vectors (GD) define the directions in which the degeneracy is lifted when moving away from the CI point.

however, involves in-plane distortions within the indole ring system. Thus, unlike the previous two conical intersections discussed, the reaction coordinate and branching space are orthogonal in this instance. The branching space is broadly similar to that of Schmitt and co-workers.[18,21]

B. UV spectra

Low resolution UV absorption spectra of indole and 5-hydroxyindole are shown in Figure 5. The indole spectrum is in good agreement with those published previously.[5–7,48] It can be seen from the spectra that the broad peak between 220 nm and 280 nm (which is predominantly due to absorption to the ^1L_a state) is approximately in the same place in both molecules, however, at wavelengths longer than 280 nm the narrower peak extending to 295 nm (due to the ^1L_b state) is seen to be significantly redshifted and broadened in the case of 5-hydroxyindole, with the absorption onset now lying close to 315 nm. Given that the ^1L_b state origins of indole and 5-hydroxyindole are known to be 283.8 nm (Refs. 8–12) and 303.9 nm,[38–40] respectively, our spectrum clearly contains significant hot-band contributions, as would be expected given the elevated temperature of the absorption cell used in our measurement. This much larger shift in the energetic position of the ^1L_b state compared to ^1L_a is consistent with our calculations (see Table I) and is also in agreement with experimental band decomposition studies carried out on the related 5-methoxyindole system in propylene glycol glass[49] and polyethylene films.[50] In Figure 5 the short wavelength feature below 220 nm in indole also appears to broaden and move to longer wavelengths in 5-hydroxyindole. This is again consistent with observations in the related 5-methoxyindole species, where both the ^1B_b and ^1B_a states are observed to undergo significant redshifts relative to their position in the indole absorption spectrum.[50]

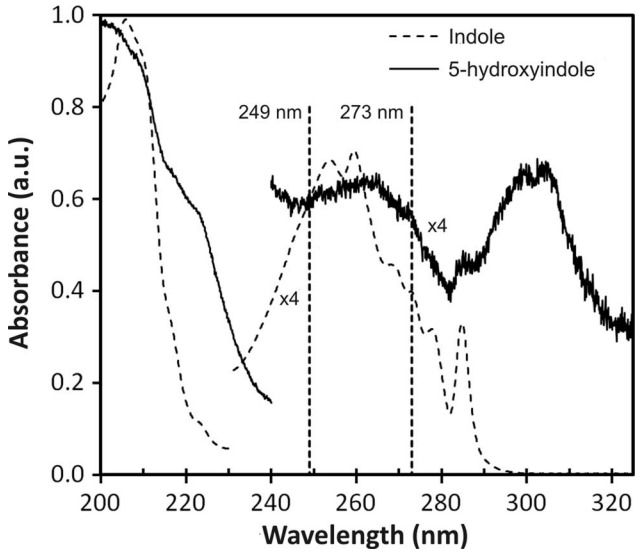

FIG. 5. Absorption spectra of indole and 5-hydroxyindole in the gas phase. Dashed vertical lines show the excitation energies used in the present study.

C. Time-resolved photoelectron spectra

We obtained time-resolved photoelectron spectra for both indole and 5-hydroxyindole at pump wavelengths centred at 249 nm and 273 nm. Indole was probed at 300 nm, which gave combined total (pump + probe) energies of 9.11 eV and 8.67 eV, respectively. 5-hydroxyindole was probed at 320 nm, giving combined total energies of 8.85 eV and 8.42 eV. The adiabatic ionisation potential for the D_0 state

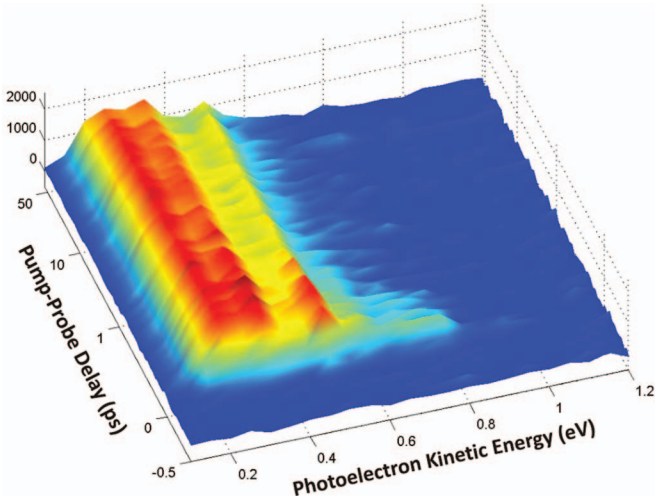

FIG. 6. Time-resolved photoelectron spectrum of indole following 249 nm excitation and subsequent ionisation with a 300 nm probe. For clarity, the time dependence is plotted using a linear scale in the region −0.5–0.5 ps and a logarithmic scale for delay times between 0.5 and 50 ps.

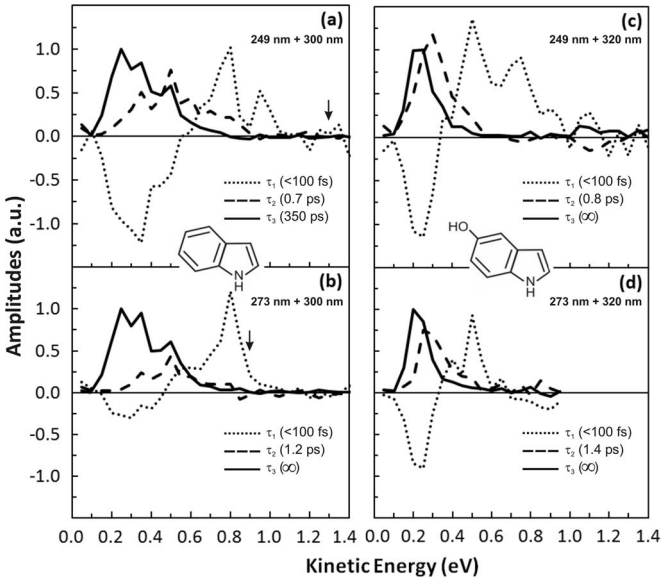

FIG. 7. Decay associated spectra (DAS) for (a) indole at 249 nm, (b) indole at 273 nm, (c) 5-hydroxyindole at 249 nm, and (d) 5-hydroxyindole at 273 nm. Numerical time constants τ_{1-3} have an uncertainty of ±20%. The individual graphs are normalised with the maximum amplitude of τ_3 set to one, and all other amplitudes then scaled relative to this. The vertical arrows on the indole data denote the maximum photoelectron energy cutoff, based on the known adiabatic ionisation potential of 7.76 eV.

of the indole cation is 7.76 eV (Refs. 51–54) and the vertical value is close to 7.9 eV.[55–58] To the best of our knowledge, the only literature data available for the D_0 ionisation potential of 5-hydroxyindole are the vertical value of 7.72 eV reported by Kubota and Kobayashi.[58] Probe wavelengths for the two molecules were chosen to give combined total energies as far above the ionisation potential as possible, without the onset of unwanted absorption of the probe by the ground state (see Figure 5). A typical data set plotting the photoelectron spectrum as a function of pump-probe delay is displayed in Figure 6 for indole following 249 nm excitation. The data are binned into 0.05 eV channels and, for clarity, the time axis is presented on a linear/logarithmic scale. A very long lived process dominates this spectrum in the 0.0–0.6 eV region, although some decaying signal, superimposed on top of this, is also evident at around 0.5 eV. Additionally, a much more rapidly decaying signal can also be observed at higher kinetic energies between 0.6 and 1.0 eV. The spectra for indole at 273 nm and for 5-hydroxyindole at both pump wavelengths used all display similar features to those seen in Figure 6, although there are some subtle differences that will be expanded upon later.

Time constants and their associated photoelectron spectra were determined using a standard Levenberg-Marquardt global fitting routine wherein the 2D data $S(E, \Delta t)$ are expressed as[59]

$$S(E, \Delta t) = \sum_i A_i(E) \cdot P_i(\Delta t) \otimes g(\Delta t). \quad (1)$$

Here $A_i(E)$ is the decay associated photoelectron spectrum of the ith data channel, which has a time dependent population $P_i(\Delta t)$, described by a series of exponentially decaying functions, and $g(\Delta t)$ is the experimentally determined Gaussian cross-correlation function. In order to non-trivially fit all data sets, three exponential functions (all originating from time-zero) were required. These time-constants were determined to be $\tau_1 < 100$ fs, $\tau_2 = 0.7$–1.4 ps, while the final time constant, τ_3, was extremely long, effectively modelling a step function over the range of pump-probe delays examined for all data sets with the exception of indole excited at 249 nm, where some decay of the long-lived signal was evident and we were able to extract a time constant of 350 ps. Although the margin of error in all of the fitted time constants is quite large (±20%), the critical advantage of the TRPES approach (when compared to "energy-integrated" experiments monitoring total ion yield as a function of pump-probe delay) is that the relative amplitude of each component in a given multi-exponential fit may be examined *as a function of electron kinetic energy*, giving rise to a series of decay associated spectra (DAS). Deconvoluting the data in this way greatly assists in the interpretation of the overall molecular dynamics since different processes, occurring on very similar timescales, may be *spectrally resolved* from each other, revealing much more information than the time constants alone. In Figures 7(a)–7(d), we present the DAS obtained from the global multiexponential fitting process outlined above. The DAS associated with each of the three time constants represent the evolution of the non-adiabatic relaxation dynamics across different electronic states. Note that the appearance of negative amplitude features in a given DAS is due to the nature of the global fitting procedure we have used, in which all exponentially decaying functions originate from zero pump-probe delay. As such, negative amplitudes effectively represent an exponential growth in photoelectron signals associated with the population of a new electronic state that was not directly accessed in the initial excitation (i.e., those signals that arise as a consequence of sequential dynamics).

IV. DISCUSSION

A. Indole at 249 nm

There have been several band decomposition studies in the UV absorption region that have been carried out on crystalline indole[60] as well as indole in propylene glycol glass[49,61,62] and polymer films.[63] On the basis of this data, we are confidently able to assume that, at 249 nm, we are exciting almost exclusively to the ^1L_a state (even given the small shifts in the relative and absolute positions of the ^1L_a and ^1L_b states in these solid media relative to the gas phase). We are therefore able to attribute the positive amplitude feature that appears between 0.6 and 1.0 eV in the DAS for τ_1, as shown in Figure 7(a), to the rapid decay of the initially prepared ^1L_a state. The negative amplitude feature in the τ_1 DAS between 0.1 and 0.6 eV represents the growth of population in new electronic states following electronic relaxation. At low photoelectron kinetic energies (<0.25 eV) the overall shape, relative amplitude and position of this feature is well matched to that of the positive DAS for the long lived feature with time constant $\tau_3 = 350$ ps. Glasser and Lami performed measurements of the collision-free, non-radiative decay rates in indole and, at 250 nm, their data suggest that the lifetime is ~180 ps, which is within a factor of 2 of our time constant τ_3.[64] It should be noted here that this work also speculated that the decrease in lifetime with increasing excitation energy was due to the ^1L_a state having electron density localised on the NH group and undergoing efficient N-H bond fission, effectively predicting the nonradiative decay mechanism which we now attribute to the $^1\pi\sigma^*$ state (*vide infra*). Our own calculations, as well as those of Sobolewski and Domcke[24–26] conclude, however, that the ^1L_a state is strongly bound along the N-H coordinate. On the basis of this evidence, and also the fact that both our calculations and those of Schmitt and co-workers[21] predict a conical intersection between the ^1L_b and ^1L_a states, we therefore suggest that, at 249 nm excitation, the τ_3 DAS originates from the ^1L_b state following extremely rapid internal conversion from ^1L_a.

The clear observation of ultrafast decay dynamics in our indole data is very different to the findings of Radloff and co-workers,[32] who observed only long lived signals in their time-resolved photoelectron spectroscopy experiments conducted at pump wavelengths of 250 nm and 263 nm. The reason for this discrepancy is not clear, although we speculate that it may be due to differences in the choice of probe scheme used in the two experiments and the associated differences in ionisation cross sections and Franck-Condon factors. The earlier work used predominantly two-photon ionisation at 400 nm, in contrast to our one-photon scheme with 300 nm.

At photoelectron kinetic energies above 0.25 eV, the agreement between the negative amplitude region of the τ_1 DAS and the τ_3 signal is clearly less good. The data therefore suggest that a second electronic state may also be populated following internal conversion from ^1L_a and that this also influences the signal present in the negative part of the τ_1 DAS. The $^1\pi\sigma^*$ state that has been previously implicated experimentally and theoretically in providing a direct dissociation pathway that leads to H atom photofragments with high kinetic energies would seem to be the obvious candidate. The work of Ashfold and co-workers has clearly observed such H atom fragments at excitation wavelengths shorter than 263 nm (Ref. 30) and so we suggest that population of this $^1\pi\sigma^*$ state, following internal conversion from ^1L_a, is also partly responsible for the observed shape of the τ_1 DAS above 0.25 eV. Since the $^1\pi\sigma^*$ state is essentially optically dark to single photon absorption, it is not accessed directly to any significant extent in the initial excitation and is populated via non-adiabatic coupling. We therefore also take the τ_2 DAS to be a direct signature of $^1\pi\sigma^*$ involvement and suggest that this is a competing mechanism with relaxation via ^1L_b. Since we do not know the relative ionisation cross sections of the ^1L_b and $^1\pi\sigma^*$ states, however, we are unable to definitively determine the branching ratio for these two pathways. The $^1\pi\sigma^*$ lifetime of 0.7 ps would appear to suggest that we are sitting just above the 0.45 eV barrier that lies along the N-H coordinate outside the Franck-Condon region (see Figure 3). We note that this lifetime is somewhat longer than might be expected, given that a system such as pyrrole exhibits a $^1\pi\sigma^*$ lifetime of <100 fs.[65] A relatively long lifetime for the indole $^1\pi\sigma^*$ state might also, however, potentially be suggested by the data of Ashfold and co-workers[30] who noted that the shape and intensity of the H atom kinetic energy release spectra they obtained were insensitive to the relative alignment of the photolysis laser polarization, implying an essentially isotropic distribution of fragment recoil velocities. At excitation wavelengths shorter than 263 nm, this includes those fast fragments arising from direct N-H dissociation on the $^1\pi\sigma^*$ surface. On the assumption that the excitation is predominantly to a single electronic state (which, as discussed earlier, we take to be the case for our data at 249 nm), this may indicate that the $^1\pi\sigma^*$ state lives long enough for the initially aligned indole molecules to de-phase to some extent. This is also in contrast to pyrrole, where anisotropic recoil of fast H-atom fragments has been observed.[66,67]

Following the population of the $^1\pi\sigma^*$ state at 249 nm the indole molecule may undergo dissociation along the N-H bond to yield an H atom and the ground state indolyl radical, as inferred from the previously discussed fast kinetic energy channels reported in studies probing either the indolyl or H atom photoproducts.[29,30] A second, alternative route is non-radiative relaxation to the vibrationally excited ground electronic state of indole. This may be followed by "statistical" fragmentation to give H atoms in conjunction with electronically excited indolyl radicals and is thought to be responsible for the slow kinetic energy channel in the frequency resolved measurements of photoproducts that have reported to date. This may occur via the proposed conical intersection between the $^1\pi\sigma^*$ and S_0 states at extended N-H bond distances, although, as will become apparent when we come to consider our data at 273 nm, we can not rule out the possibility of other, additional pathways. A third potential outcome for the $^1\pi\sigma^*$ state may, in principle, involve internal conversion to the ^1L_b state. If this were the case, however, then we might expect to see some form of signal appearing in the photoelectron spectrum with a rise time that matched the $^1\pi\sigma^*$ decay lifetime. The fact that we see no such signals leads us to conclude that this pathway is not of major significance, although we note that, in the event of the $^1\pi\sigma^*$ state possessing a much larger

ionisation cross section than the ^1L_b state, we may be effectively "blind" to such a process. The lack of a rising signal anywhere in the data that are matched to the decay of the τ_2 DAS also leads us to rule out the possibility of the τ_2 DAS being due to the second step in a bi-exponential decay of the ^1L_a state (that then relaxes exclusively to ^1L_b), rather than the $^1\pi\sigma^*$ state.

Finally, we also note that the ultimate fate of the ^1L_b state, which we observe to decay on a timescale of several hundred picoseconds following internal conversion from ^1L_a, remains unclear. Since the fluorescence quantum yield is relatively low ($\phi \sim 0.1$) (Ref. 64) there must be an, as yet uncharacterised, non-radiative decay pathway for this state. It is interesting to speculate that this may, in fact, be an additional source of the "statistical" H atoms that have been previously observed in frequency resolved studies of the dissociation products. Our measurements also show no obvious evidence of triplet states being accessed via intersystem crossing, as suggested by the time-resolved electron diffraction data of Zewail and co-workers.[33] The data reported by this group quote a rise time of 6.3 ps for the population of a (subsequently long lived) state following excitation at 267 nm. However, our TRPES data exhibit no signals with comparable dynamical timescales. Even if our experiment was effectively "blind" to the triplet state itself due to an unfavourable ionisation cross section, we suggest that observation of a decaying signal in some region of the photoelectron spectrum might be expected due to disappearing population in the state from which any triplet state is being populated.

We now turn our attention back the τ_1 DAS in Figure 7(a). Unlike the DAS for τ_2 and τ_3, which we take to be direct representations of the photoelectron spectra associated with ionisation from the $^1\pi\sigma^*$ state and ^1L_b state, respectively, the τ_1 DAS is not a true representation of the photoelectron spectrum associated with the ^1L_a state. This is due to the nature of the global fitting procedure we have used to analyse the data, which assumes that all exponentially decaying signals originate from zero pump-probe delay. As such, the fit introduces negative amplitudes into the τ_1 DAS in order to compensate for photoelectron signals that originate from electronic states populated following internal conversion after the initial excitation. However, since we have determined that the population of both the ^1L_b and $^1\pi\sigma^*$ states originates directly from the initially prepared ^1L_a state we are, in this particular instance, able to extract the true ^1L_a photoelectron spectrum by adding together the DAS for the three individual time constants used in the fit. This has the effect of isolating the component of the τ_1 DAS associated exclusively with the decay of the ^1L_a state, given the previously discussed assumption that there is no significant excitation directly to the ^1L_b state at 249 nm. The result of this operation is shown in Figure 8. In addition to the peaks at 0.8 eV and 0.95 eV that were visible in the original τ_1 DAS in Figure 7(a), a new feature at 0.5 eV, that was previously obscured, is now also readily apparent. At 249 nm excitation, we are sitting 0.44 eV above the proposed ^1L_a origin and the total (pump + probe) energy available is 9.11 eV. Given that the ^1L_a state originates from the HOMO (and so is expected to ionise predominantly into the D_0 state of the indole cation), and taking the vertical ionisation potential of 7.9 eV reported in the He(I) photoelectron spectrum of indole,[55–58] we would therefore predict a peak corresponding to diagonal ionisation (i.e., $\Delta v = 0$, where v is a generalised, non-mode-specific quantum number) to appear at close to 0.8 eV in the τ_1 DAS. This is what we indeed observe. The smaller features at 0.95 eV and 0.5 eV also provide some indication of ionisation events for which $\Delta v \neq 0$, although the absence of a long progression extending all the way to the maximum photoelectron energy cutoff (which is 1.35 eV in this instance) would suggest no major changes in geometry upon ionisation. Additionally, in the case of ionisation from the ^1L_b state, we are sitting 0.61 eV above the ^1L_b origin following ^1L_a excitation at 249 nm and subsequent internal conversion. Given that the ^1L_b state originates from the HOMO-1 orbital, diagonal ionisation into the D_1 state of the indole cation (which is known to lie at 8.36 eV (Refs. 55–58)) would therefore be expected to give rise to a strong feature close to 0.15 eV in the τ_3 DAS. This is not observed, although we note that the transmission efficiency of our spectrometer decreases sharply at very low photoelectron kinetic energies. We are therefore unable to comment further on the nature of the ^1L_b ionisation.

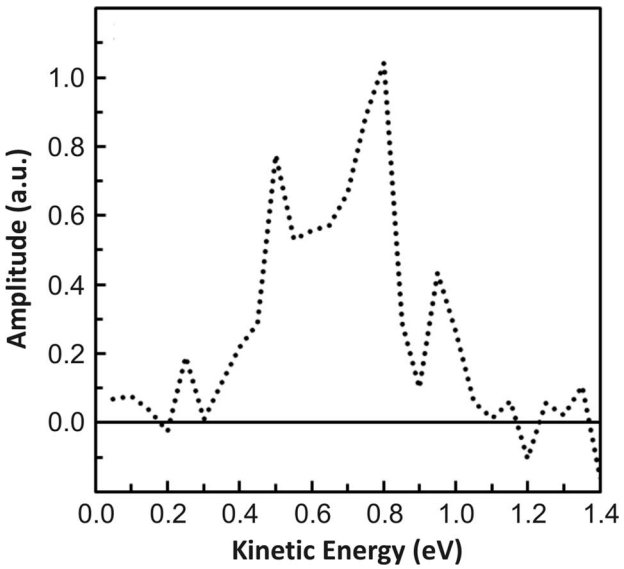

FIG. 8. Sum of the three individual decay associated spectra (DAS) presented in Figure 7(a) for indole excited at 249 nm. For more details, see the main text.

B. Indole at 273 nm

The three DAS obtained for indole at an excitation wavelength of 273 nm are shown in Figure 7(b). The general appearance of this data is very similar to that seen at 249 nm and it is interesting to note that the spectral features in all three DAS appear at the same photoelectron kinetic energies for both excitation wavelengths. This observation suggests that the nature of the ionisation event is very similar following excitation at the two wavelengths, with the additional 0.44 eV of internal energy deposited into the ^1L_a state upon 249 nm excitation (relative to 273 nm) being directly mapped into the indole cation. The total (pump + probe) energy available in

this instance is 8.67 eV. Once again taking the vertical ionisation potential of 7.9 eV, we would predict the $\Delta v = 0$ photoelectron peak to appear at close 0.8 eV in the τ_1 DAS, as is observed. The $\Delta v < 0$ peak at 0.95 eV in the 249 nm data is not present at 273 nm as we are exciting at the ^1L_a origin. The spectral positions of all other features in the three DAS at 273 nm are essentially identical to those observed at 249 nm.

There are also several other important points to take from a comparison of Figures 7(a) and 7(b). Firstly, at 273 nm we still see a clear signature of decay via the $^1\pi\sigma^*$ state, which we have attributed to the τ_2 DAS, providing direct evidence that this state is involved in the relaxation dynamics at longer wavelengths than the 263 nm threshold for the production of fast H atom fragments observed by Ashfold and co-workers.[30] This observation represents a good example of the complementary nature of time- and frequency-resolved measurements: The observation of fast H atom fragments at wavelengths shorter than 263 nm allows us to definitively assign the τ_2 DAS in our data at 249 nm to the $^1\pi\sigma^*$ state. The appearance of this same τ_2 DAS at 273 nm then allows us to subsequently assign a role to the $^1\pi\sigma^*$ state in the indole relaxation dynamics below the fast H-atom threshold. Secondly, the time constant τ_2 is longer at 273 nm than at 249 nm (1.2 ps vs. 0.7 ps). This is significant as the magnitude of this increase is larger then anything that can simply be attributed to the uncertainty of our fitting procedure, although the timescale of the decay is still sufficiently short to suggest that tunnelling through the barrier along the N-H coordinate is unlikely to be a prevailing pathway. This is particularly apparent given that 273 nm corresponds to a reduction in excitation energy of 0.44 eV compared to 249 nm, although the decay rate is less than a factor of 2 slower. The $^1\pi\sigma^*$ state is therefore unable to decay via internal conversion to the S_0 state along the N-H coordinate as the relevant conical intersection lies at an extended distance, on the other side of the barrier (see Figure 3). An alternative decay pathway, mediated by a different vibrational mode, must therefore be responsible. In order to investigate this possibility further, we performed constrained conical intersection searches at a variety of restricted N-H distances, however, we were unable to find any points of degeneracy between the $^1\pi\sigma^*$ state and the S_0 state under these conditions and so the nature of any alternative radiationless decay pathway at short N-H distances remains an open question.

An additional point of note in Figure 7(b) is that the relative amplitudes of the features associated with the three time constants are clearly different to those observed at 249 nm. In particular, the negative amplitude feature in the τ_1 DAS is significantly smaller following excitation at 273 nm. Although this could, in part, be a consequence of the different Franck-Condon factors involved in the ionisation step following excitation at the two different wavelengths, at around 273 nm, the indole fluorescence excitation spectrum exhibits a well resolved vibronic band structure characteristic of direct excitation to a long lived state. Data reported by several groups show a cluster of several sharp peaks in the region between 272 and 274 nm and these are thought to be ^1L_b vibronic states that derive their intensity through Herzberg-Teller vibronic coupling with ^1L_a.[11,19,20] The broad bandwidth ($\sim$150 cm^{-1} FWHM) of the ultrafast pulses used in our experiments will excite all of these states simultaneously and, as such, some contribution to the signal described by the τ_3 DAS will now be from direct excitation to these ^1L_b state vibronic bands and will therefore originate from zero pump-probe delay.

Finally, in contrast to the situation at 249 nm excitation, we are unable to extract a lifetime for the τ_3 DAS at 273 nm as it is essentially a step function over the range of pump-probe delays employed in our measurements ($\Delta t_{max} = 50$ ps). This is consistent with the observations of Glasser and Lami,[64] whose data suggest a lifetime (for what we now take to be the ^1L_b state) on the order of several nanoseconds for indole excited close to the proposed ^1L_a origin.

C. 5-hydroxyindole at 249 nm and 273 nm

The data obtained for 5-hydroxyindole, shown in Figures 7(c) and 7(d), appear to demonstrate broadly similar dynamics to those observed in indole, both in terms of the spectral content of the various DAS as well as the dynamical timescales. We therefore conclude that 5-hydroxyindole exhibits similar electronic relaxation mechanisms to those observed in indole, with non-adiabatic coupling occurring between the initially prepared ^1L_a state and both the ^1L_b and $^1\pi\sigma^*$ states. The 5-hydroxyindole molecule may potentially dissociate not only along the N-H bond, but also along the O-H bond of the hydroxyl group. There are, therefore, also two potential routes for relaxation back to the ground electronic state and/or H atom elimination. At a purely heuristic level, it would therefore seem reasonable to assume that the dynamical timescales and/or relative amplitudes and spectral features of the three DAS we obtain for 5-hydroxyindole at a given excitation wavelength should be significantly altered, relative to the case of indole, if such additional pathways were present. The fact that they are not leads us to conclude that the presence of OH group in 5-hydroxyindole does not play a major role in the relaxation dynamics at the two excitation wavelengths used in our present study. This is consistent with the recent findings of Ashfold and co-workers,[40] who have suggested that the OH group in 5-hydroxyindole is a spectator in the relaxation process due to the nature of the interaction between the O atom p_x orbital and the π system of the indole ring, with the relative destabilizing contributions of this orbital to the HOMO and HOMO-1 being the key consideration.

There are a number of additional points in Figures 7(c) and 7(d) that warrant further consideration. Firstly, in contrast to indole, we do not see such a dramatic reduction in the amplitude of the negative portion of the τ_1 DAS in 5-hydroxyindole at 273 nm excitation when compared to 249 nm. As discussed previously, the ^1L_b state in 5-hydroxyindole experiences a significant redshift relative to its position in indole and therefore less direct excitation to this state might be expected to occur at 273 nm. As such, a smaller signal level in the τ_3 DAS (associated with ionisation of the ^1L_b state) will therefore originate from zero pump-probe delay. Secondly, at both excitation wavelengths used in our study we were unable to extract a numerical time constant τ_3 for 5-hydroxyindole given the limited ($\leq$50 ps) range of pump-probe delays that were sampled. Once again turning

to the non-radiative lifetime study of Glasser and Lami,[64] we note that this would seem to be broadly consistent with the observation of lifetimes on the order of 1 ns that were reported for the related 5-methoxyindole species at both 273 nm and 249 nm. Finally, it is interesting to note that Sobolewski and Domcke have reported an *ab initio* dynamical study on the photochemistry of the related 5,6-dihydroxyindole molecule. These authors proposed that the initially excited $^1\pi\pi^*$ state(s) may relax non-adiabatically via the $^1\pi\sigma^*_{OH}$ state leading to hydrogen migration to the neighbouring carbon atom of the six-membered ring.[68] This forms a structure denoted 6-hydroxy-4-dihydro-indol-5-one (HHI), that is predicted to absorb strongly in the visible region of the spectrum, undergoing a transition to an excited state of $^1\pi\pi^*$ character which then rapidly relaxes back to the HHI ground state. It was suggested that this overall process may play an important role in the photoprotection provided by the eumelanin system. In principle, a similar mechanism might also be possible in 5-hydroxyindole, although we note that the HHI system may receive additional stabilization from the interaction between the two oxygen atoms (via the H atom of the OH group attached to the 6 position) that would obviously be absent in the mono-hydroxylated system. The migration of an H-atom onto the 6-membered ring will induce significant changes in the geometry of the molecular framework and this should be dramatically reflected in the appearance of the photoelectron spectra we see. The very similar nature of the data we have obtained for indole and 5-hydroxyindole leads us to speculate that, at the excitation wavelengths we have employed, this H atom migration mechanism is not significant in 5-hydroxyindole.

V. CONCLUSION

We have investigated the non-adiabatic relaxation dynamics of indole and 5-hydroxyindole at excitation wavelengths of 249 nm and 273 nm using time-resolved photoelectron spectroscopy. We observe the two systems to exhibit similar behaviour and at both excitation wavelengths used, with the initially prepared ^1L_a state decaying on an "ultrafast" (<100 fs) timescale via either the ^1L_b state or the $^1\pi\sigma^*$ state. This is in contrast to some previous time-resolved studies performed on indole where the involvement of $^1\pi\sigma^*$ state has not been observed and the $^1L_a/^1L_b$ relaxation dynamics were not deconvoluted. The involvement of the $^1\pi\sigma^*$ state in the dynamics at 249 nm is consistent with the data from frequency-resolved experiments interrogating the kinetic energy release distribution of photoproducts. We are also able to directly observe the role of the $^1\pi\sigma^*$ state at considerably longer wavelengths than has been inferred previously. The similarity of the dynamics observed in indole and 5-hydroxyindole at both excitation wavelengths leads us to conclude that the role of the OH group in 5-hydroxyindole is minimal. This observation is also consistent with very recent frequency-resolved studies.

ACKNOWLEDGMENTS

The authors are grateful for the financial support of EPSRC and NRC. D.T. would also like to thank G. M. Roberts, V. G. Stavros, A. Longarte, and T. A. A. Oliver for helpful discussions. O.S. thanks the Humbolt foundation for a research fellowship. LTB and MJP would like to acknowledge the support of the European Research Council under the European Union's Seventh Framework Programme grant FR/2007-2013/ERC Grant no. 258990.

[1] P. Meredith and T. Sarna, Pigm. Cell Res. **19**, 572 (2006).
[2] P. Meredith, B. J. Powell, J. Reisz, S. P. Nighswander-Rempel, M. R. Pederson, and E. G. Moore, Soft Matter **2**, 37 (2006).
[3] A. Huijser, A. Pezzella, and V. Sundström, Phys. Chem. Chem. Phys. **13**, 9119 (2011).
[4] J. R. Platt, J. Chem. Phys. **17**, 484 (1949).
[5] H. Lami, J. Chem. Phys. **67**, 3274 (1977).
[6] H. Lami, Chem. Phys. Lett. **48**, 447 (1977).
[7] P. Ilich, Can. J. Spectrosc. **32**, 19 (1987).
[8] J. M. Hollas, Spectrochim. Acta **19**, 753 (1963).
[9] J. Hager and S. C. Wallace, J. Phys. Chem. **87**, 2121 (1983).
[10] Y. Nibu, H. Abe, N. Mikami, and M. Ito, J. Phys. Chem. **87**, 3898 (1983).
[11] R. Bersohn, U. Even, and J. Jortner, J. Chem. Phys. **80**, 1050 (1984).
[12] J. W. Hager, D. R. Demmer, and S. C. Wallace, J. Phys. Chem. **91**, 1375 (1987).
[13] G. A. Bickel, D. R. Demmer, A. E. Outhouse, and S. C. Wallace, J. Chem. Phys. **91**, 6013 (1989).
[14] D. M. Sammeth, S. Yan, L. H. Spangler, and P. R. Callis, J. Phys. Chem. **94**, 7340 (1990).
[15] J. R. Cable, J. Chem. Phys. **92**, 1627 (1990).
[16] T. L. O. Bartis, L. I. Grace, T. M. Dunn, and D. M. Lubman, J. Phys. Chem. **97**, 5820 (1993).
[17] G. Berden, W. L. Meerts, and E. Jalviste, J. Chem. Phys. **103**, 9596 (1995).
[18] J. Küpper, D. W. Pratt, W. L. Meerts, C. Brand, J. Tatchen, and M. Schmitt, Phys. Chem. Chem. Phys. **12**, 4980 (2010).
[19] B. J. Fender, D. M. Sammeth, and P. R. Callis, Chem. Phys. Lett. **239**, 31 (1995).
[20] V. A. Povedailo and D. L. Yakovlev, J. Appl. Spectrosc. **75**, 336 (2008).
[21] C. Brand, J. Küpper, D. W. Pratt, W. L. Meerts, D. Krügler, J. Tatchen, and M. Schmitt, Phys. Chem. Chem. Phys. **12**, 4968 (2010).
[22] M. N. R. Ashfold, G. A. King, D. Murdock, M. G. D. Nix, T. A. A. Oliver, and A. G. Sage, Phys. Chem. Chem. Phys. **12**, 1218 (2010).
[23] L. Serrano-Andrés and B. O. Roos, J. Am. Chem. Soc. **118**, 185 (1996).
[24] A. L. Sobolewski and W. Domcke, Chem. Phys. Lett. **315**, 293 (1999).
[25] A. L. Sobolewski, W. Domcke, C. Dedonder-Lardeux, and C. Jouvet, Phys. Chem. Chem. Phys. **4**, 1093 (2002).
[26] A. L. Sobolewski and W. Domcke, J. Phys. Chem. A **111**, 11725 (2007).
[27] A. L. Sobolewski and W. Domcke, Chem. Phys. **259**, 181 (2000).
[28] B. C. Dian, A. Longarte, and T. S. Zwier, J. Chem. Phys. **118**, 2696 (2003).
[29] M.-F. Lin, C.-M. Tseng, Y. T. Lee, and C.-K. Ni, J. Chem. Phys. **123**, 124303 (2005).
[30] M. G. D. Nix, A. L. Devine, B. Cronin, and M. N. R. Ashfold, Phys. Chem. Chem. Phys. **8**, 2610 (2006).
[31] A. Iqbal and V. G. Stavros, J. Phys. Chem. A **114**, 68 (2010).
[32] H. Lippert, H.-H. Ritze, I. V. Hertel, and W. Radloff, Chem. Phys. Lett. **398**, 526 (2004).
[33] S.-T. Park, A. Gahlmann, Y. He, J. S. Feenstra, and A. H. Zewail, Angew. Chem. Int. Ed. **47**, 9496 (2008).
[34] M. A. El-Sayed, J. Chem. Phys. **38**, 2834 (1963).
[35] J. Catalán, P. Perez, and A. U. Acuña, J. Mol. Struct. **142**, 179 (1986).
[36] D. Robinson, N. A. Besley, E. A. M. Lunt, P. O'Shea, and J. D. Hirst, J. Phys. Chem. B **113**, 2535 (2009).
[37] S. Arnold, L. Tong, and M. Sulkes, J. Phys. Chem. **98**, 2325 (1994).
[38] Y. Huang and M. Sulkes, Chem. Phys. Lett. **254**, 242 (1996).
[39] M. Sulkes and I. Borthwick, Chem. Phys. Lett. **279**, 315 (1997).
[40] T. A. A. Oliver, G. A. King, and M. N. R. Ashfold, Phys. Chem. Chem. Phys. **13**, 14646 (2011).
[41] P. Kruit and F. H. Read, J. Phys. E: Sci. Instrum. **16**, 313 (1983).
[42] S. Lochbrunner, J. J. Larsen, J. P. Shaffer, M. Schmitt, T. Schultz, J. G. Underwood, and A. Stolow, J. Electron. Spectrosc. Relat. Phenom. **112**, 183 (2000).
[43] U. Even, J. Jortner, D. Noy, N. Lavie, and C. Cossart-Magos, J. Chem. Phys. **112**, 8068 (2000).
[44] J. F. Stanton and R. J. Bartlett, J. Chem. Phys. **98**, 7029 (1993).
[45] O. Christiansen, H. Koch, and P. Jørgensen, J. Chem. Phys. **105**, 1451 (1996).

[46]M. J. Frisch, G. W. Trucks, H. B. Schlegel *et al.*, GAUSSIAN 09, Revision A.02, Gaussian Inc., Wallingford, CT, 2009.
[47]DALTON, Release 2.0, a molecular electronic structure program, 2005, see http://www.kjemi.uio.no/software/dalton/dalton.html.
[48]N. A. Borisevich and T. F. Raichuyonok, Dokl. Phys. **52**, 405 (2007).
[49]M. R. Eftink, L. A. Selvidge, P. R. Callis, and A. A. Rehms, J. Phys. Chem. **94**, 3469 (1990).
[50]B. Albinsson and B. Nordén, J. Phys. Chem. **96**, 6204 (1992).
[51]J. Hager, M. Ivanco, M. A. Smith, and S. C. Wallace, Chem. Phys. Lett. **113**, 503 (1985).
[52]T. Vondrák, S. Sato, and K. Kimura, J. Phys. Chem. A **101**, 2384 (1997).
[53]J. E. Braun, T. L. Grebner, and H. J. Nuesser, J. Phys. Chem. A **102**, 3273 (1998).
[54]M. de Groot, J. Broos, and W. J. Buma, J. Chem. Phys. **126**, 204312 (2007).
[55]J. H. D. Eland, Int. J. Mass Spectrom. Ion Phys. **2**, 471 (1969).
[56]L. J. Dolby, G. Hanson, and T. Koenig, J. Org. Chem. **41**, 3537 (1976).
[57]L. N. Domelsmith, L. L. Munchausen, and K. N. Houk, J. Am. Chem. Soc. **99**, 4311 (1977).
[58]M. Kubota and T. Kobayashi, J. Electron. Spectrosc. Relat. Phenom. **128**, 165 (2003).
[59]O. Schalk, A. E. Boguslavskiy, and A. Stolow, J. Phys. Chem. A **114**, 4058 (2010).
[60]Y. Yamamoto and J. Tanaka, Bull. Chem. Soc. Jpn. **45**, 1362 (1972).
[61]B. Valeur and G. Weber, Photochem. Photobiol. **25**, 441 (1977).
[62]R. L. Rich, Y. Chen, D. Neven, M. Négrerie, F. Gai, and J. W. Petrich, J. Phys. Chem. **97**, 1781 (1993).
[63]E. Jalviste and N. Ohta, J. Chem. Phys. **121**, 4730 (2004).
[64]N. Glasser and H. Lami, J. Chem. Phys. **74**, 6526 (1981).
[65]H. Lippert, H.-H. Ritze, I. V. Hertel, and W. Radloff, ChemPhysChem **5**, 1423 (2004).
[66]J. Wei, A. Kuczmann, J. Riedel, F. Renth, and F. Temps, Phys. Chem. Chem. Phys. **5**, 315 (2003).
[67]B. Cronin, M. G. D. Nix, R. H. Qadiri, and M. N. R. Ashfold, Phys. Chem. Chem. Phys. **6**, 5031 (2004).
[68]A. L. Sobolewski and W. Domcke, ChemPhysChem **8**, 756 (2007).